Journal of the Meteorological Society of Japan, Vol. 73, No. 4, pp. 817–826, 1995

NOTES AND CORRESPONDENCE

A Transient CO_2 Experiment with the MRI CGCM

—Quick Report—

By Tatsushi Tokioka[1], Akira Noda, Akio Kitoh, Yoshinobu Nikaidou, Shinji Nakagawa, Tatsuo Motoi, Seiji Yukimoto

Meteorological Research Institute, Tsukuba, Ibaraki 305, Japan

and

Kumiko Takata[2]

Engineering Research Center, Tokyo Electric Power Company, Chofu, Tokyo 182, Japan

(Manuscript received 10 September 1994, in revised form 12 June 1995)

Abstract

A transient response experiment to the gradual increase in atmospheric CO_2 concentration at a compound rate of 1 %/yr has been performed with a coupled atmosphere-ocean general circulation model (CGCM) developed at the Meteorological Research Institute (MRI). The model is characterized by two aspects; one is a relatively high resolution of the oceanic part in the low latitudes to simulate El Niño phenomena, and the other is an elaborate sea ice model to simulate seasonal variation of sea ice coverage and thickness.

Time integration has been performed up to 70 years over which the CO_2 concentration doubles. The globally averaged surface air temperature increases 1.6°C during this period. Atmospheric response to the CO_2 increase is slow in the Southern Hemisphere and over oceanic areas. However, the surface air temperature increase in the high latitudes in the Northern Hemisphere is not dominant up to the year 50. This speed of CO_2-induced warming is affected by interdecadal variation of sea ice found both in the transient and in the control runs. It is also suggested that leads in sea ice act as a strong negative feedback on changes in sea ice volume, affecting the timing of the warming.

Analysis of sea surface temperature shows that the dominant air-sea coupled mode in the model is very close to what is observed. This mode shows interannual variations in the Pacific with a dominant period of about 6 years, which is close to the typical time scale of El Niño. It also shows variations of interdecadal time scales, with implication of predictability for a few decades.

1. Introduction

Transient response studies to a gradual increase in atmospheric CO_2 have been reported by four groups so far (IPCC, 1992). They are by GFDL (Stouffer *et al.*, 1989; Manabe *et al.*, 1991; Manabe *et al.*, 1992; Delworth *et al.*, 1993), NCAR (Washington and Meehl, 1989; Meehl *et al.*, 1993), UKMO (Murphy, 1992) and MPI (Cubasch *et al.*, 1992). None of these models have fine enough horizontal resolutions of ocean to simulate El Niño phenomena, although Neelin (1991) has shown that the coarse-grid coupled models are simulating an unstable coupled mode that contributes to some of the ENSO signal. There are debates on how El Niño phenomena change under global warming. The GFDL group shows that the amplitude of sea surface temperature (SST) anomalies during ENSO-like events in the CO_2-warmed climate is slightly reduced compared to that in the control run (Knutson and Manabe,

1 Present affiliation: Japan Meteorological Agency, Tokyo 100, Japan

2 Present affiliation: Center for Climate System Research, University of Tokyo, Tokyo 153, Japan

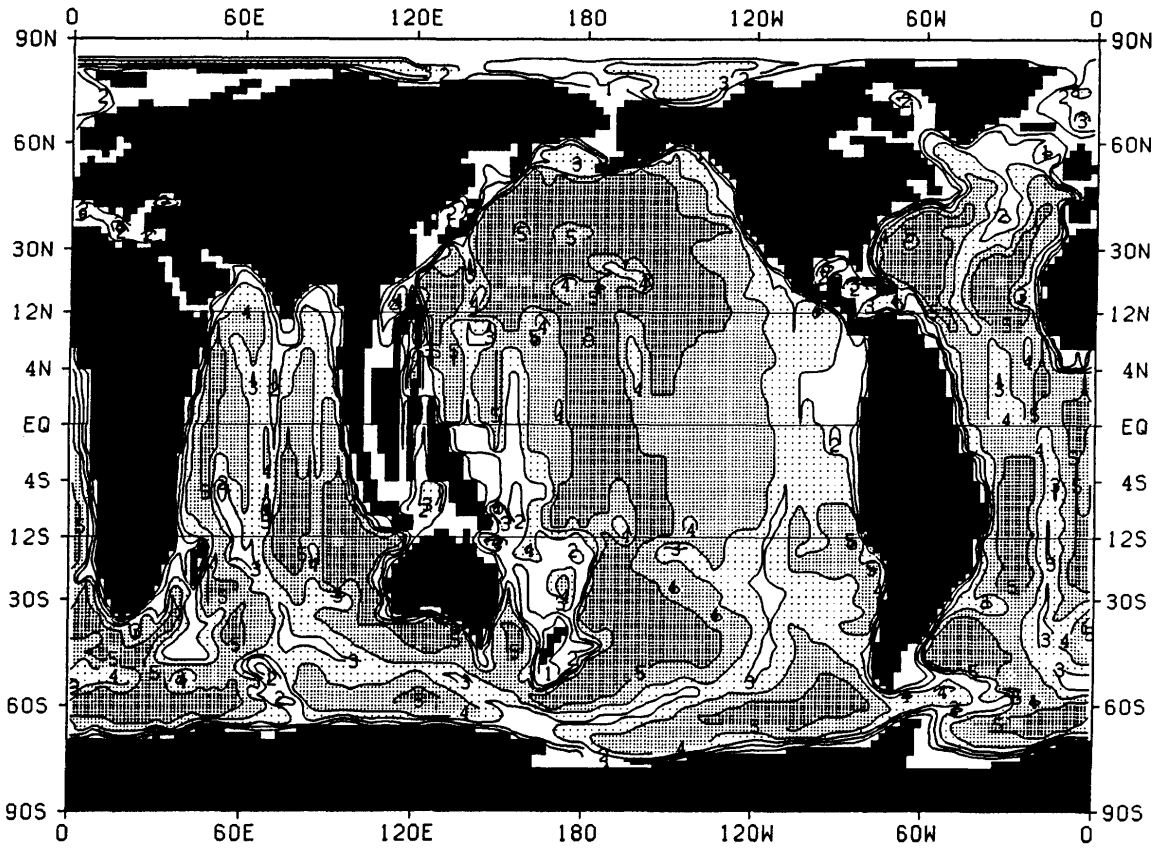

Fig. 1. The horizontal resolution and topography of the OGCM. Variable resolution is used in the meridional direction, ranging from 0.5° at the equator to 2.0° at 12° latitude and further poleward. The contour interval is 1000 m

1994). The MPI group also speculates less active El Niño under the warming process (Lunkeit *et al.*, 1993), while the NCAR group shows that there is no significant change in SST variability with increased CO_2, but there is enhanced precipitation variability (Meehl *et al.*, 1993). On the other hand, the UKMO group shows no significant changes in the equatorial SST variability between the transient and control simulations (Tett, 1994). However, these models have not successfully simulated the whole cycle of El Niño phenomena well. Unless we perform simulations of transient response to the gradual increase in CO_2 with a model which simulates them better than so far, no convincing conclusion can be reached.

Some models used for transient response studies do not simulate either sea ice thickness or its distribution well. In one model, sea ice thickness in the Antarctic ocean in September is more than 3 m in some area (Manabe *et al.*, 1992). However, observation shows that thickness of the sea ice in the Antarctic ocean is 40–60 cm in austral midwinter (Wadhams *et al.*, 1987). In another model, sea ice in the Antarctic ocean has almost disappeared, even in September (Murphy, 1992). If a model does not simulate either thickness or distribution of sea ice or both of them well, it is quite likely that the model fails to evaluate feedback processes related to sea ice quantitatively, and produces some errors in predicting possible future climate changes due to the increase in CO_2.

In this quick report, we describe results of a simulation of transient response to the gradual increase in CO_2 with a climate model which has been improved in the aspects mentioned above. Full description of the present results will be presented later in separate reports.

2. Model

The atmospheric part of the model (AGCM) is identical to that used for the Atmospheric Model Intercomparison Project (AMIP) and its performance is described in Kitoh *et al.* (1995). Horizontal resolution of the AGCM is 5° by 4° in longitudinal and latitudinal directions, respectively. There are 15 vertical levels with a top at 1 hPa. Short-wave radiation calculation is based on Lacis and Hansen (1974) and long-wave radiation calculation on Shibata and Aoki (1989). Five types of clouds are diagnostically determined: *i.e.*, penetrative cumulus cloud, middle level convective cloud, planetary

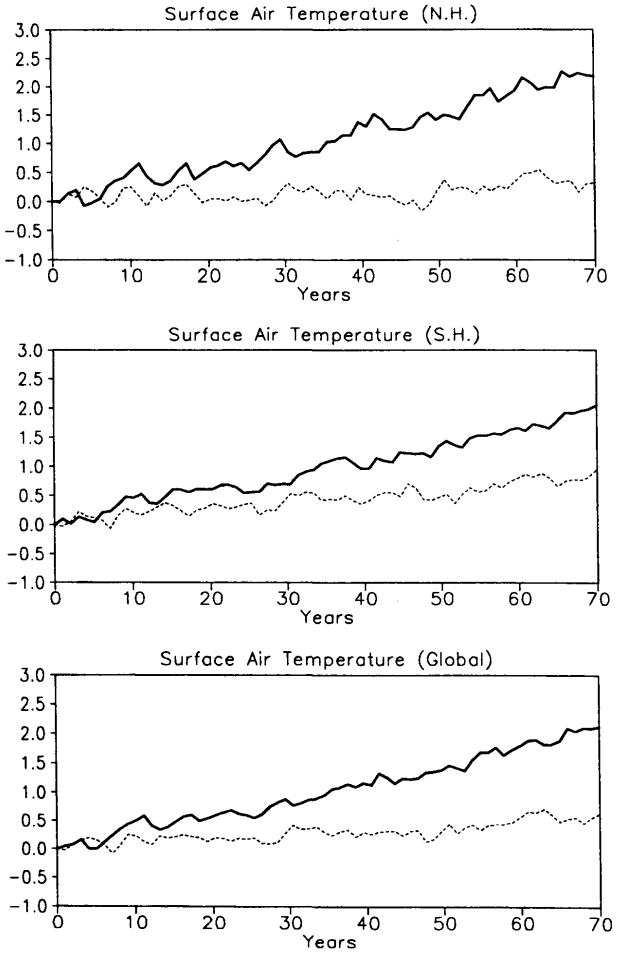

Fig. 2. Time evolution of annual-mean surface air temperature averaged over the Northern Hemisphere (top), the Southern Hemisphere (middle) and the globe (bottom). Solid and dashed lines indicate the G run and the C run, respectively. The zero point is the annual mean for the first year of the C run. In the G run, CO_2 concentration is increased at a compound rate of 1 %/yr, while it is fixed in the C run.

boundary layer stratus cloud, large-scale condensation cloud and cirrus anvil cloud. Partial cloudiness is allowed for the convective clouds. Effect of subgrid-scale topography on the grid-scale flow is included as gravity-wave drag following Palmer *et al.* (1986), with quantitative adjustment described by Yagai and Yamazaki (1988). Thermodynamic and hydrological processes of land surface are based on a multi-layer soil model. There are four layers with a bottom at 10 m depth. Ground temperature, soil moisture and frozen soil moisture are predicted at each level.

The oceanic part of the model (OGCM) is a global ocean general circulation model developed at the Meteorological Research Institute (MRI) (see Nagai *et al.*, 1992). The model is now extended to include a realistic ocean bottom topography and a variable resolution in the meridional direction, ranging from 0.5° at the equator to 2.0° at 12° latitude and further poleward (see Fig. 1). The resolution in the longitudinal direction is 2.5° and there are 21 vertical layers, 11 of which are located in the first 300 m. The Mellor-Yamada level 2 turbulence closure scheme is included to simulate the oceanic mixed layer. The lateral eddy viscosity and diffusivity are set to 2.0×10^9 cm^2/s and 5.0×10^7 cm^2/s, respectively, between 78°N and 78°S. The vertical eddy viscosity and diffusivity are calculated following Mellor and Yamada (1974, 1982) and Mellor and Durbin (1975).

A sea ice model is included. The model predicts compactness (areal coverage ratio of sea ice) as well as thickness and surface temperature of sea ice. The movement of sea ice is predicted by considering advection due to oceanic current at the first level of the ocean. The thermodynamics of sea ice is parameterized following Mellor and Kantha (1989). Energy exchanges through the surface are calculated both in the sea ice area and "leads" separately and are weighted with the respective coverage ratio. The model can simulate seasonal variations of sea ice compactness and thickness realistically not only in the Arctic but also in the circum-Antarctic area. The performances of the sea ice model will be described fully in a separate paper.

The climate model used has different horizontal resolution between the AGCM and the OGCM. Furthermore, we predict areal coverage ratio of sea ice in each ocean grid, as explained above. We calculate the surface energy fluxes in one atmospheric grid as the sum of area-weighted energy fluxes between the atmosphere and the underlying surface component (which is either land, open ocean or sea ice) within the atmosphere grid. We allow partial coverage of land at both coastal and island grids.

3. Experiment

The ocean was spun up with an acceleration method for 1500 years from an isothermal motionless state with a uniform salinity. Then a time integration was made for 30 years by coupling the AGCM with the OGCM, to obtain flux corrections in the surface energy and water fluxes. In these runs, SST and sea surface salinity (SSS) were relaxed to observed climatological fields (Levitus, 1982).

Two runs were performed, *i.e.*, a run with a fixed atmospheric CO_2 concentration (C run) at 345 ppmv and a run with a gradual increase in CO_2 at a compound rate of 1 %/yr (G run). This increasing rate of CO_2 roughly corresponds to the actual increase of radiative forcing due to the increase in several greenhouse gases and has been used in other

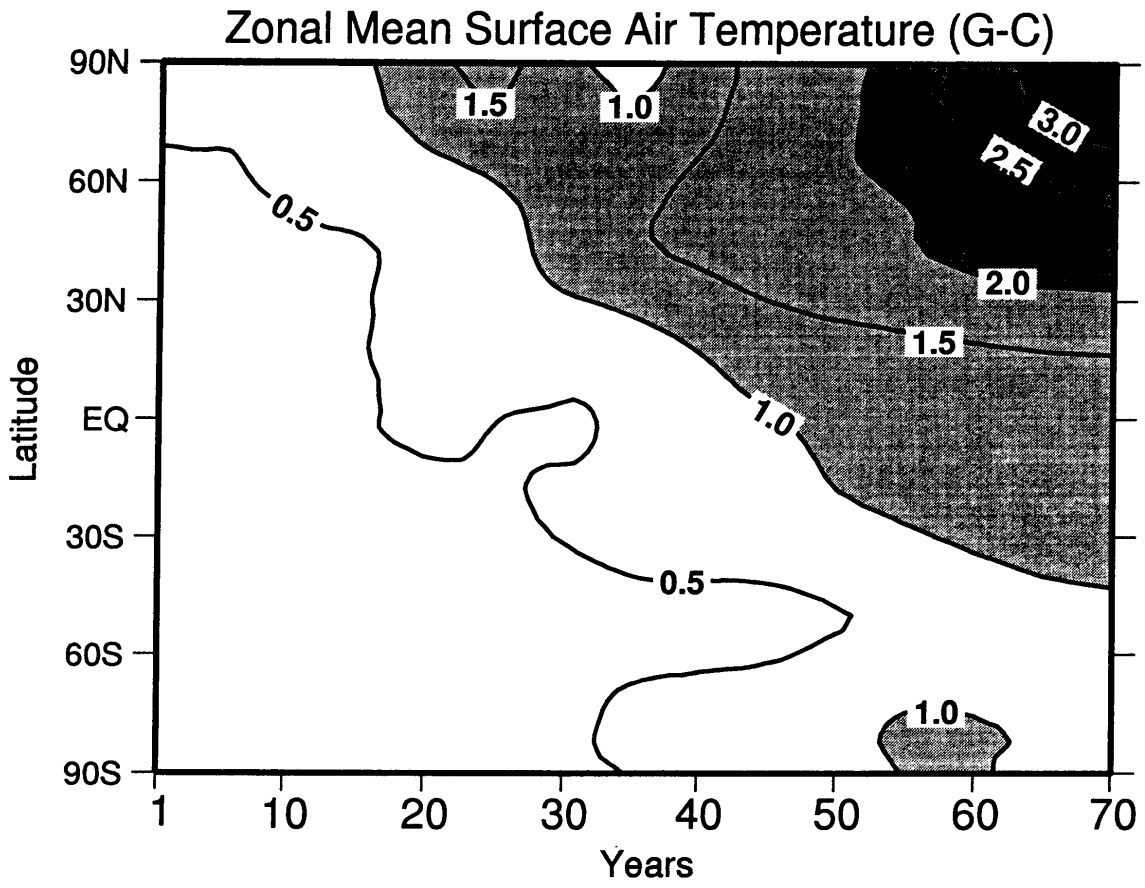

Fig. 3. Latitude-time section of zonally averaged surface air temperature difference, which is taken between the G run and the C run at the same time instance. Periods shorter than 12 years have been filtered out.

studies (Stouffer *et al.*, 1989; Manabe *et al.*, 1991; Murphy, 1992). In both C and G runs the flux corrections in the surface energy and water fluxes were included to predict realistic SST and surface salinity. Runs were continued up to the year 70 in both C and G runs.

4. Results

In this paper, most analyses will be based on the difference between the G run and the C run (G-C). The C run has succeeded in reproducing not only basic climatological characteristics of time mean fields including SST but also variabilities in from interannual to interdecadal time scales.

4.1 Global mean temperature

Figure 2 shows the time evolution of the area-averaged, annual-mean surface air temperature for the C run and the G run. There remains a weak secular trend in the Southern Hemisphere in the C run, which is, however, smaller than the CO_2 warming signal. The globally averaged surface air temperature difference, G-C, increases by 1.6°C during the seventy-year period.

Murphy (1992) and Cubasch *et al.* (1992) have mentioned initial slow rise in the globally averaged surface air temperature in relation to the initial spin-up problem or the cold start problem (Hasselmann

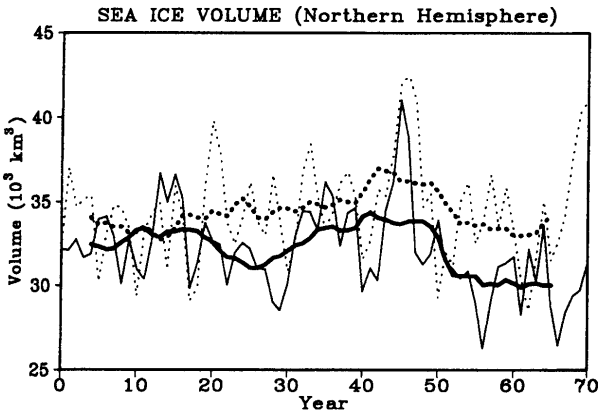

Fig. 4. Temporal variation of sea ice volume (10^3 km^3) in the Northern Hemisphere for the G run (solid lines) and the C run (dotted lines). Thin and thick lines indicate annual mean and 11-year running mean, respectively.

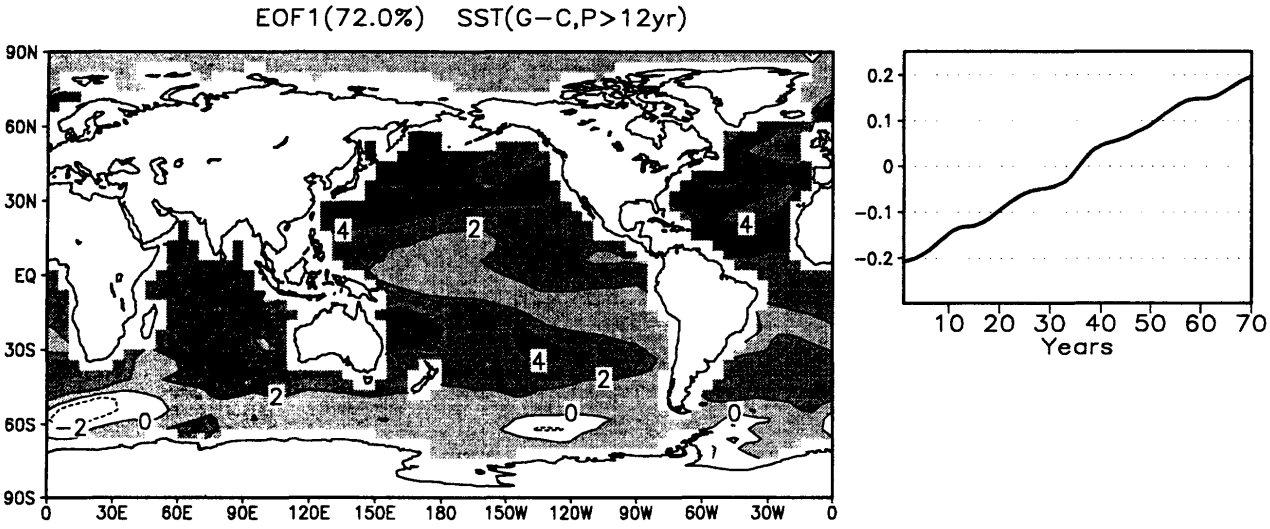

Fig. 5. The first mode of empirical orthogonal function (EOF) analysis of the annually averaged sea surface temperature (SST) difference between the G run and the C run. (right) Spatial pattern, (left) time evolution of the amplitude of the mode. Periods shorter than 12 years have been filtered out. Contribution of this mode is shown in the parentheses at the top of the figure.

et al., 1992). However, in our experiment, the globally averaged surface air temperature increases almost linearly, as shown in Fig. 2.

4.2 Zonal mean temperature and sea ice

Figure 3 shows the latitude-time section of zonally averaged surface air temperature change. The delay of temperature rise in the Southern Hemisphere, especially around 50°S, is dominant, as already pointed out by Stouffer *et al.* (1989). It is also worthy to note that the rise of surface air temperature in the Arctic region is rather small up to the year 50. However, it starts to increase at a higher rate after the year 50. This has not been stressed before although a similar tendency is seen in Fig. 1 of Stouffer *et al.* (1989) and Fig. 1 of Meehl *et al.* (1993).

Figure 4 shows the temporal variation of sea ice volume in the Northern Hemisphere for the C and G runs. It can be seen that there are interdecadal variations as well as interannual variations in the simulated sea ice volume, and that the interdecadal variations have amplitudes comparable to those due to the doubled CO_2 radiative forcing around the year 70. This indicates that the temporal evolution of CO_2 warming in the northern high latitudes is much affected by not only the amplitude but also the phase of the natural variability in sea ice. In the present experiment, a transition from the positive to the negative anomaly phase in sea ice volume happens to be around the year 50, so that a delay (acceleration) of the warming is found before (after) that time. This ice variability may be indicative of some kind of global low-frequency variability that is most readily manifested by the sea ice.

Although the temperature increase is dominant in high latitudes of the Northern Hemisphere, it is not so large compared with the result at GFDL (Stouffer *et al.*, 1989). The increase occurs mostly in the last 20 years, as shown in Fig. 3. In the present model, sensible and latent heat fluxes from leads increase in proportion to the increase of area of leads when the SST increases. This works as a negative feedback to the SST rise. Another negative feedback works in sea ice region because heat conduction increases as ice thickness decreases. However, the feedback in the lead region is much stronger than that in the sea ice region. The difference in the magnitude of the negative feedback may partly be responsible for the smaller temperature rise in the Arctic in the present simulation than in the GFDL's where no lead is considered in the sea ice model.

4.3 EOF analysis

Figure 5 shows the spatial pattern of the first mode of the empirical orthogonal function (EOF) analysis for the annual mean SST difference (G-C) and the time variation of the coefficient. Temporal variations shorter than 12 years have been filtered out for the SST difference. The first EOF of SST of the G run is almost identical to that shown in Fig. 5 for G-C. The coefficient shows an overall linear increasing trend over 70 years, indicating that this is a response mode to the gradual increase in CO_2. The SST rise is large in the sea of Okhotsk as the sea ice has partially disappeared. This is expected from the fact that the area is located near the southernmost boundary of sea ice formation in the Northern Hemisphere, so that the sea ice-albedo feedback may work early and effectively. Between 40°S and 60°S

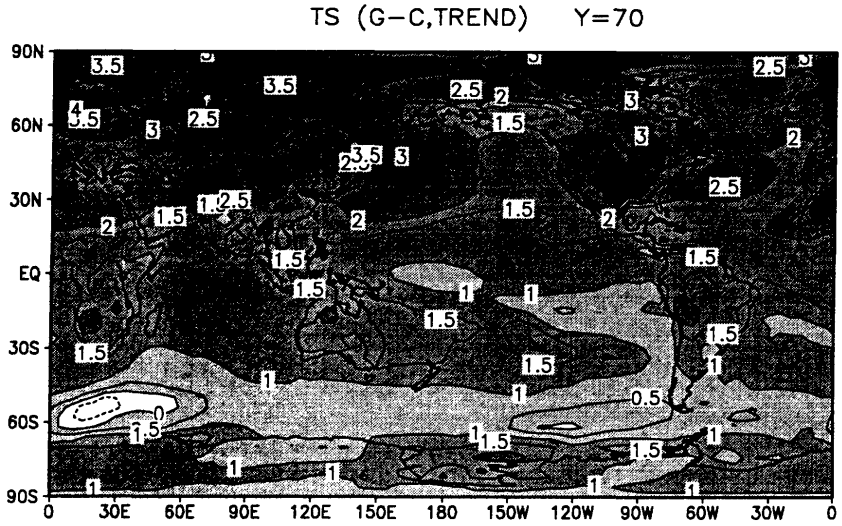

Fig. 6. The increase in surface air temperature during 70 years estimated from a linear regression of the temperature difference G-C.

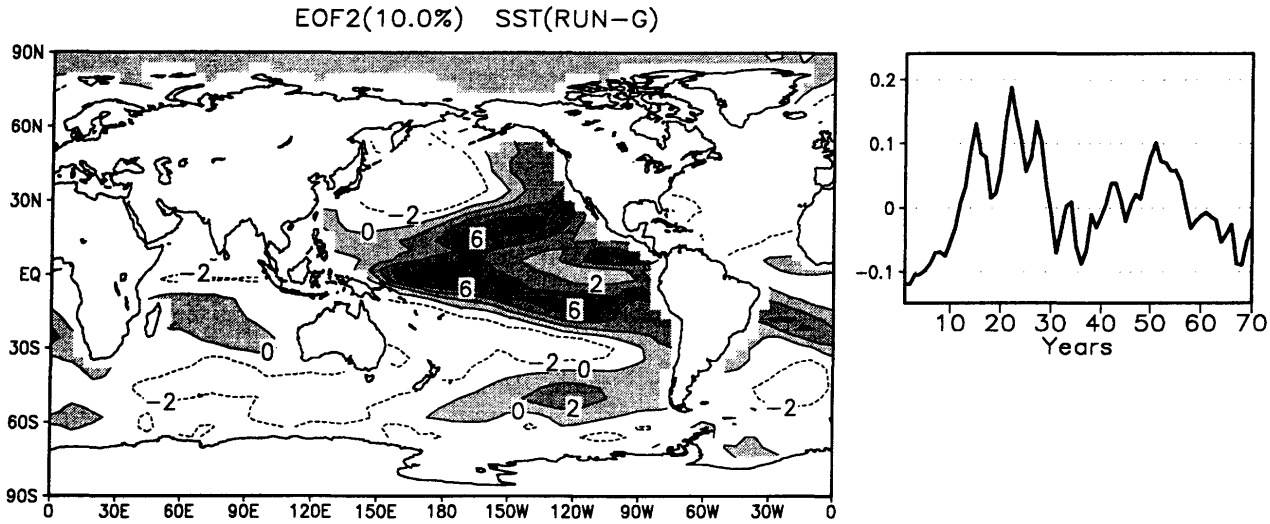

Fig. 7. The second mode of EOF analysis of the annually averaged SST for the G run. No low-pass filter has been applied.

where most area is covered by ocean, the SST rise is generally delayed as in other studies (Stouffer *et al.*, 1989; Murphy, 1992; Cubasch *et al.*, 1992; Meehl *et al.*, 1993). There is dominant warming in the North Pacific, the North Atlantic and the subtropical latitudes of the Southern Hemisphere. The warming in the North Atlantic may reflect the fact that the meridional circulation in the North Atlantic is weak in the present experiment.

Figure 6 shows the spatial pattern of the increase in annual mean surface air temperature during 70 years estimated from a linear regression of the temperature difference G-C. As is expected, the spatial pattern in Fig. 6 is almost identical to that in Fig. 5 over the ocean. There are pronounced increases in temperature over the continent in mid-latitudes in both hemispheres. This land-sea contrast of the warming is explained by Saito and Tokioka (1994). The most dominant increase is found over the sea of Okhotsk due to the disappearance of sea ice, as mentioned above.

Figure 7 is the second EOF of SST for the G run. This mode has large amplitudes in the Pacific. The most notable feature is a wedge like pattern in the central Pacific, with an opposite polarity in the north-western and the south-western mid Pacific. An almost identical spatial pattern is observed in the first EOF for the C run, as shown in Fig. 8, indicating that this is an internal mode of the climate system. A similar correspondence between the first

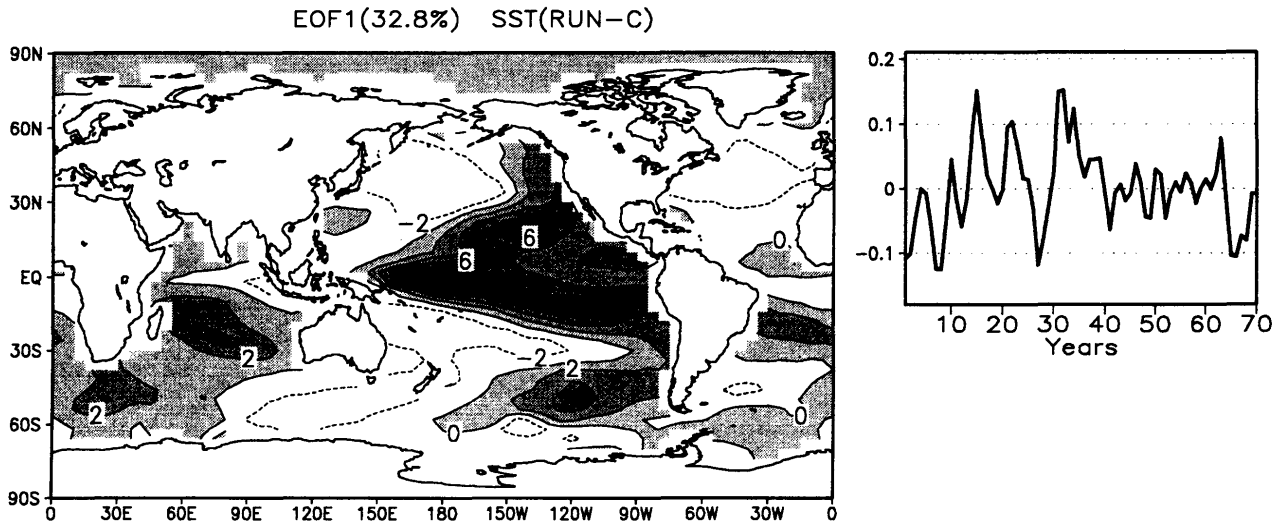

Fig. 8. The same as in Fig. 7, but for the first EOF of the SST for the C run.

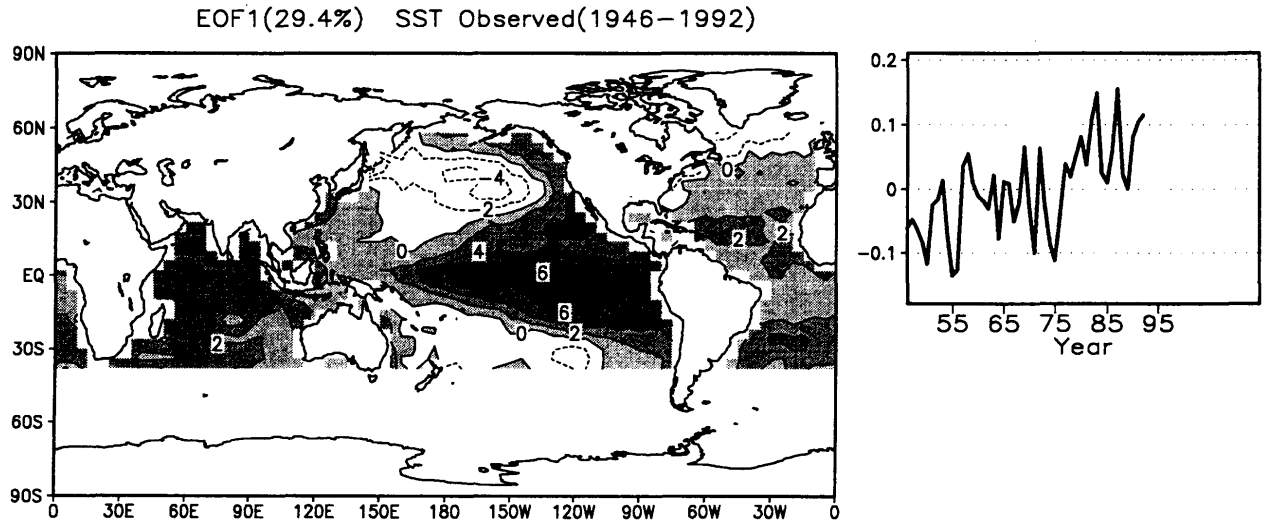

Fig. 9. The same as in Fig. 7, but for the first EOF for the observed SST, which is a combination of COADS data from 1946 to 1985 and the JMA analysis from 1986 to 1992.

EOF for the control run and the second EOF for the transient CO_2 run is found in Fig. 12 of Cubasch *et al.* (1992), although the spatial pattern of the mode is different from that for the present experiment. It can be seen in Figs. 7 and 8 that the coefficients of these two EOFs show dominant 6-year cycles, which is close to the typical time scale of El Niño, and interdecadal modulations of them of about 30 years. Another important point to be noted is that the interdecadal time evolutions of both modes are almost identical to each other up to the year 30 or so. This type of variation could be little affected by the increase in CO_2 concentration, and thus could be predicted about 30 years ahead. The mechanisms of the variability of this mode is being studied and will be reported separately from this study. This mode has a characteristic structure in the Pacific sub-tropical gyre down to about 500 m depth, which will be the main reason for the long time predictability of over 30 years.

Figure 9 shows the first EOF of the observed annually averaged SST data, which are combinations of the COADS data (before 1985) and the JMA analyses (after 1986). Figure 9 has several common characteristic features to those of Figs. 7 and 8. As the time evolution in Fig. 9 shows, there is a kind of jump in the latter half of 1970s. Before this, it remains negative. However, it remains positive thereafter. Above-normal SST in the eastern equatorial Pacific, and below-normal SST in the Northern mid Pacific observed in recent years are captured by this mode.

Quick comparison of variability in the El Niño time scale between time evolutions of Figs. 7 and 8 does not show clear differences. Here, we do not make any conclusive statements on the change of El Niño phenomena due to the increase in CO_2. This point will be studied further, separately.

5. Concluding remarks

A coupled atmosphere-ocean general circulation model has been developed. The model is characterized by two aspects; one is a relatively high resolution of the oceanic part in low latitudes to simulate El Niño phenomena, and the other is an elaborate sea ice model to simulate seasonal variation of sea ice coverage and thickness. A transient response experiment to the gradual increase in atmospheric CO_2 concentration at a compound rate of 1 %/yr has been performed. We have focused on topics relevant to these aspects in this report. Other topics and model performance will be presented in detail elsewhere.

Time integration has been performed using flux corrections in the surface energy and water fluxes up to 70 years, when the CO_2 concentration has doubled. Not only the sea ice volume as shown in Fig. 4 but also its extent, distribution and thickness have stayed stable during the time integration, and such a systematic sea ice drift as in Cubasch *et al.* (1994) is not found in the present experiment. However, the interdecadal sea ice variability is evident both in the C and G runs. This low frequency variability is coupled with the constantly increasing CO_2 radiative forcing to affect the timing of the rapid warming after the year 50. The speed of CO_2-induced warming in high latitudes in the Northern Hemisphere in the present experiment is slower than those obtained by the GFDL group (Stouffer *et al.*, 1989) where lead is not considered in the sea ice model. This suggests that the negative feedback effect of lead on sea ice change may be playing an important role in determing the warming speed.

The ENSO-like phenomena have been simulated both in the C and G runs. Analysis of SST shows that the most dominant air-sea coupled mode in the model is very close to what is observed. The most notable feature is a wedge like pattern in the central Pacific, with an opposite polarity in the northwestern and the south-western mid Pacific. This mode shows interannual variations in the Pacific with a dominant period of about 6 years, which is close to the typical time scale of El Niño. It also shows variations of interdecadal time scales, with implication of predictability over a few decades. Although no definite indication is found that the ENSO is affected by the CO_2-induced warming, the present study suggests that the low-frequency variability interacts with CO_2-induced climate changes. The sea ice variability presented in this report may be indicative of some kind of global low-frequency variability that is mostly readily manifested by the sea ice.

Acknowledgments

The present study was performed as a part of the special study on the prediction of global warming sponsored by the Japan Meteorological Agency. A part of this study was supported also by the Center for Global Environmental Research/ National Institute for Environmental Studies.

References

Cubasch, U., K. Hasselmann, H. Höck, E. Maier-Reimer, U. Mikolajewicz, B.D. Santer and R. Sausen, 1992: Time-dependent greenhouse warming computations with a coupled ocean-atmosphere model. *Clim. Dyn.* **8**, 55–69.

Delworth, T., S. Manabe and R.J. Stouffer, 1993: Interdecadal variations of the thermohaline circulation in a coupled ocean-atmosphere model. *J.Climate*, **6**, 1993–2011.

Hasselmann, K., R. Sausen, E. Maier-Reimer and R. Voss, 1992: On the cold start problem of coupled atmosphere-ocean models. MPI Report No. 83, MPI, Hamburg, 25pp.

IPCC, 1992: Climate Change 1992; *The Supplementary Report to the IPCC Scientific Assessment.* Eds. J.T. Houghton, B.A. Callander and S.K. Varney, Cambridge Univ. Press, 200pp.

Kitoh, A., A. Noda, Y. Nikaidou, T. Ose and T. Tokioka, 1995: AMIP simulations of the MRI GCM. *Pap. Meteor. Geophys.*, **45**, (in press).

Knutson, T.R. and S. Manabe, 1994: Impact of increasing CO_2 on the Walker Circulation and ENSO-like phenomena in a coupled ocean-atmosphere model. *Extended Abstracts of the Sixth Conference on Climate Variations*, 23–28 January 1994, Nashville, 80–81.

Lacis, A.A. and J.E. Hansen, 1974: A parameterization for the absorption of solar radiation in the Earth's atmosphere. *J. Atmos. Sci.*, **31**, 118–133.

Levitus, S., 1982: Climatological Atlas of the World Oceans, *NOAA Prof. Pap.*, **13**, U.S. Government Printing Office, Washington, D.C.

Lunkeit, F., R. Sausen and J.M. Oberhuber, 1993: Simulation of the transient greenhouse warming with the coupled atmosphere-ocean model ECHAM2/OPYC. *Abstracts of IAMAP·IAHS '93*, 11–23 July, 1993, Yokohama, M3-66.

Manabe, S., R.J. Stouffer, M.J. Spelman and K. Bryan, 1991: Transient responses of a coupled ocean-atmosphere model to gradual changes of atmospheric CO_2. Part I: Annual mean response. *J. Climate*, **4**, 785–818.

Manabe, S., M.J. Spelman and R.J. Stouffer, 1992: Transient response of a coupled ocean-atmosphere model to gradual changes of atmospheric CO_2. Part II: Seasonal response. *J. Climate*, **5**, 105–126.

Meehl, G.A., G.W. Branstator and W.M. Washington, 1993: Tropical Pacific interannual variability and CO_2 climate change, *J. Climate.*, **6**, 42–63.

Mellor, G.L. and P.A. Durbin, 1975: The structure and dynamics of the ocean surface mixed layer. *J. Phys. Oceanogr.*, **5**, 718–728.

Mellor, G. L and L. Kantha, 1989: An ice-ocean coupled model. *J. Geophys. Res.*, **94**, 10,937–10,954.

Mellor, G.L. and T. Yamada, 1974: A hierarchy of turbulence closure models for planetary boundary layers. *J. Atmos. Sci.*, **31**, 1791–1806.

Mellor, G.L. and T. Yamada, 1982: Development of a turbulence closure model for geophysical fluid problems. *Rev. Geophys. Space Phys.*, **20**, 851–875.

Murphy, J.M., 1992: A prediction of the transient response of climate. *Climate Res. Tech. Note*, No. 32, Hadley Centre.

Nagai, T., T. Tokioka, M. Endoh and Y. Kitamura, 1992: El Niño-Southern Oscillation simulated in an MRI atmosphere-ocean coupled general circulation model. *J. Climate*, **5**, 1202–1233.

Neelin, J.D., 1991: The slow sea surface temperature mode and the fast-wave limit: analytical theory for tropical interannual oscillations and experiments in a hybrid coupled model. *J. Atmos. Sci.*, **48**, 584–606.

Palmer, T.N., G.J. Shutts and R. Swinbank, 1986: Alleviation of a systematic westerly bias in general circulation and numerical weather prediction models through an orographic gravity wave drag parameterization. *Quart. J. Roy. Meteor. Soc.*, **112**, 1001–1039.

Saito, M. and T. Tokioka, 1994: Some aspects of ocean/continental-scale climate changes under global warming produced by CO_2 increase. *Extended Abstracts of the Sixth Conference on Climate Variations*, 23–28 January 1994, Nashville, 82–86.

Shibata, K. and T. Aoki, 1989: An infrared radiative scheme for the numerical models of weather and climate. *J. Geophys. Res.*, **94**, 14,923–14,943.

Stouffer, R.J., S. Manabe and K. Bryan, 1989: Interhemispheric asymmetry in climate response to a gradual increase of atmospheric CO_2. *Nature*, **342**, 660–662.

Tett, S.F.B., 1994: Simulation of El Niño/Southern Oscillation like variability in a global AOGCM and its response to CO_2 increase. *Climate Res. Tech. Note*, No. 45, Hadley Centre.

Wadhams, P., M.A. Lange and S.F. Ackley, 1987: The ice thickness distribution across the Atlantic Sector of the Antarctic Ocean in midwinter. *J. Geophys. Res.*, **92**, 14,535–14,552.

Washington, W.M. and G.A. Meehl, 1989: Climate sensitivity due to increased CO_2 experiments with a coupled atmosphere and ocean general circulation model. *Clim. Dyn.*, **4**, 1–38.

Yagai, I. and K. Yamazaki, 1988: Effect of the internal gravity wave drag on the 12-layer MRI GCM January simulation. *Report No. 12 of the Proceedings of the WGNE Workshop on Systematic Errors in Models of the Atmosphere*, 19–23 September 1988, Working Group on Numerical Experimentation, Toronto, 8pp.

気象研究所大気海洋結合モデルによる CO_2 漸増実験 —速報—

時岡達志[1]・野田　彰・鬼頭昭雄・二階堂義信・中川慎治・本井達夫・行本誠史

(気象研究所気候研究部)

高田久美子[2]

(東京電力株式会社技術研究所)

気象研究所で開発された大気海洋結合モデルを用いて、大気中の CO_2 を年率 1% (複利) で増加させる CO_2 漸増実験を行った。モデルの特徴として、第一に、エルニーニョ現象を再現するために低緯度で高い解像度が用いられている点、第二に、観測に近い海氷の分布及び厚さを再現するために改良された海氷モデルが用いられている点があげられる。

CO_2 濃度が倍増する 70 年間にわたり積分をおこなった。この間に全球年平均地上気温は 1.6°C 増加した。CO_2 増加に対する大気の応答は南半球及び海洋で遅れがみられた。しかし、北半球高緯度では 50 年後まであまり大きな地上気温の上昇がみられなかった。二酸化炭素の増加によって引き起こされる北半球高緯度での温暖化のスピードはコントロールラン、漸増ランの両方においてみられた海氷の数十年スケールの変動に影響されていることが示された。更に、海氷中の氷の割れ目 (リード) が海氷体積の変動に対して強い負のフィードバック作用を持つことが温暖化に影響を与えることが示唆された。

[1]現在所属：気象庁予報部長期予報課

[2]現在所属：東京大学気候システム研究センター

海面水温の変動の解析から、モデルで最も卓越する大気海洋結合モードとして、観測から解析されたものと非常によく似たものがえられた。このモードは、太平洋で卓越し、年々変動に約6年の卓越周期がみられ、これはエルニーニョの典型的時間スケールに近いものである。更に、このモードは数十年スケールでも変動しており、変動が二、三十年間予測可能であることを示唆している。